Miner Deposita (2012) 47:653–662
DOI 10.1007/s00126-011-0328-9

ARTICLE

Mineralogy and geochemistry of gold-bearing arsenian pyrite from the Shuiyindong Carlin-type gold deposit, Guizhou, China: implications for gold depositional processes

Wenchao Su · Hongtao Zhang · Ruizhong Hu · Xi Ge · Bin Xia · Yanyan Chen · Chen Zhu

Received: 26 September 2010 / Accepted: 6 January 2011 / Published online: 29 January 2011

Abstract Arsenian pyrite in the Shuiyindong Carlin-type gold deposit in Guizhou, China, is the major host for gold with 300 to 4,000 ppm Au and 0.65 to 14.1 wt.% As. Electron miroprobe data show a negative correlation of As and S in arsenian pyrite, which is consistent with the substitution of As for S in the pyrite structure. The relatively homogeneous distribution of gold in arsenian pyrite and a positive correlation of As and Au, with Au/As ratios below the solubility limit of gold in arsenian pyrite, suggest that invisible gold is likely present as Au^{1+} in a structurally bound Au complex in arsenian pyrite. Geochemical modeling using the laser ablation-inductively coupled plasma mass spectrometry (LA-ICP-MS) analysis of fluid inclusions for the major ore forming stage shows that the dominant Au species were $Au(HS)_2^-$ (77%) and $AuHS_{(aq)}^0$ (23%). Gold-hydroxyl and Gold-chloride complexes were negligible. The ore fluid was undersaturated with respect to native Au, with a saturation index of −3.8. The predominant As species was $H_3AsO_3^0{}_{(aq)}$. Pyrite in the Shuiyindong deposit shows chemical zonation with rims richer in As and Au than cores, reflecting the chemical evolution of the ore-bearing fluids. The early ore fluids had relatively high activities of As and Au, to deposit unzoned and zoned arsenian pyrite that host most gold in the deposit. The ore fluids then became depleted in Au and As and formed As-poor pyrite overgrowth rims on gold-bearing arsenian pyrite. Arsenopyrite overgrowth aggregates on arsenian pyrite indicate a late fluid with relatively high activity of As. The lack of evidence of boiling and the low iron content of fluid inclusions in quartz, suggest that iron in arsenian pyrite was most likely derived from dissolution of ferroan minerals in the host rocks, with sulfidation of the dissolved iron by H_2S-rich ore fluids being the most important mechanism of gold deposition in the Shuiyindong Carlin-type deposit.

Keywords Gold · Arsenian pyrite · Carlin-type · Shuiyindong · Guizhou · China

Editorial handling: B. Lehmann

Electronic supplementary material The online version of this article (doi:10.1007/s00126-011-0328-9) contains supplementary material, which is available to authorized users.

W. Su (✉) · R. Hu · X. Ge
State Key Laboratory of Ore Deposit Geochemistry, Institute of Geochemistry, Chinese Academy of Sciences,
Guiyang 550002, China
e-mail: suwenchao@vip.gyig.ac.cn

H. Zhang
Key laboratory of Virtual Geographic Environment, Nanjing Normal University,
Nanjing 210046, China

B. Xia
School of Marine Sciences, Sun Yat-Sen University,
Guangzhou 510275, China

Y. Chen · C. Zhu
Department of Geological Sciences, Indiana University,
Bloomington, IN, USA

Introduction

Sediment-hosted gold deposits, also known as Carlin-type gold deposits, are well-known for their invisible gold (Simon et al. 1999a). Various studies have documented that gold in the primary ores is hosted largely by arsenian pyrite (300–9,000 ppm Au, Reich et al. 2005), and that gold in arsenian pyrite occurs as a substituting cation in the pyrite solid solution (Au^{1+}) and/or as nanoparticles of native gold (Au^0) (Bakken et al. 1989; Cook and Chryssoulis 1990; Mao 1991; Fleet et al. 1993, 1997; Simon et al. 1999a, b;

Hofstra and Cline 2000; Cline 2001; Emsbo et al. 2003; Zhou and Wang 2003; Palenik et al. 2004; Reich et al. 2005). Au^{1-} and Au^{3+} also have been suggested to occur in pyrite solid solution (Arehart et al. 1993; Li et al. 2003). The understanding of the chemical state of gold in iron sulfides is important for mineral processing of refractory sulfide ores and for the understanding of gold depositional processes in Carlin-type deposits.

Shuiyindong is one of the largest (~100 tonnes with average gold grade of 5 ppm) stratabound Carlin-type gold deposits in China. It is hosted in Permian bioclastic limestone that contains disseminated pyrite and arsenopyrite. Previous electron microprobe analysis (EMPA) studies have shown that gold is predominantly in arsenian pyrite (500 to 6,000 ppm Au), with lesser amounts in arsenopyrite (800 ppm Au) (Fu et al. 2004). Native gold in arsenian pyrite was reported by Su et al. (2008). Modal analyses show that most gold occurs as "invisible" gold in iron sulfides (~95%), with subordinate free native gold (~5%, Liu 2003). We here present new mineralogical and geochemical data for arsenian pyrite and arsenopyrite from the Shuiyindong Carlin-type gold deposit using ore petrography, permanganate staining technique, and EMPA to evaluate the relation between gold grades and pyrite textures, the chemical characteristics of gold in arsenian pyrite, and to discuss the depositional processes of gold.

Geological setting

The Shuiyindong mine, approximately 20 km northwest of the town of Zhenfeng in Guizhou, China, is located at the southwestern margin of the Precambrian Yangtze craton (Fig. 1a). It is hosted in Permian bioclastic limestone near the axis of the Huijiabao anticline. Recent exploration and underground mining at Shuiyindong has proven gold reserves of 100 tonnes Au, with average gold grade of 5 ppm. All gold is contained in refractory ores in which arsenian pyrite is the major host mineral. The geology of the deposit was described in Su et al. (2008).

The sedimentary rocks in the district consist of bioclastic limestone, siltstone, and argillite of Permian and Triassic age. These rocks form the nearly E–W trending Huijiabao anticline with a known length of about 20 km. The anticline is cut by reverse faults, striking E–W and dipping steeply to the north and south, respectively (Fig. 1b). A series of nearly S–N trending normal faults cuts the reverse faults, commonly controlling mercury-thallium deposits, such as

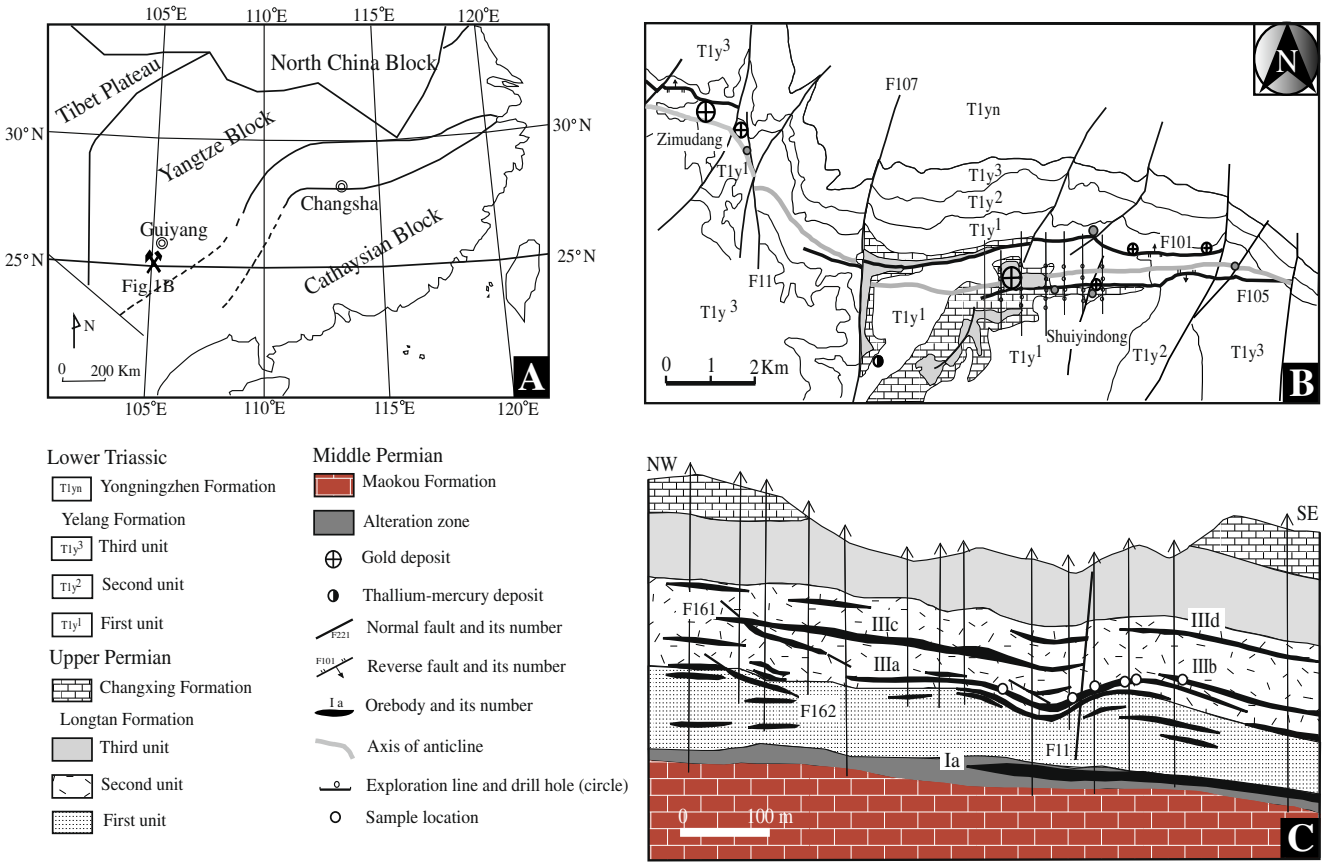

Fig. 1 Geological plan and cross section of the Shuiyindong gold deposit. Modified from Liu 2001

Lanmuchang (Fig. 1b). Gold mineralization occurs mainly on the flanks of the anticline and is preferentially disseminated in bioclastic limestone and calcareous siltstone of the first and second units of the Upper Permian Longtan Formation at depths of 100 to 900 m below the surface (Fig. 1c). Lower grade ore bodies are hosted in silicified, brecciated argillite and limestone at the unconformity between the Middle Permian Maokou massive limestone and the first unit of the Longtan Formation, and in reverse faults with realgar and orpiment bodies.

The country rocks are commonly affected by decarbonation, silicification, sulfidation and dolomitization. Sulfides in the deposit are mainly arsenian pyrite, arsenopyrite, and marcasite with minor orpiment, realgar, and stibnite. Gangue minerals include quartz, dolomite, calcite, and clay minerals (e.g., kaolinite).

Gold mineralization and paragenesis

The samples used in this study were collected from two main orebodies, IIIa and IIIb, at a depth of 200 m below the surface (Fig. 1c). These samples contain 10 to 100 ppm Au, and consist of arsenian pyrite and arsenopyrite disseminated in a matrix of ferroan calcite, dolomite, and quartz. Gold mineralization is closely associated with decarbonation, silicification, sulfidation and dolomitization, similar to the situation in Nevada, USA (Hofstra and Cline 2000). Decarbonation of limestone is evident from small relict inclusions of calcite to dolomite in quartz (Hofstra and Cline 2000). Silicification is characterized by quartz crystals commonly containing small relicts of ferroan calcite and dolomite inclusions (Fig. 2b, d), which are similar to those of jasperoid quartz (Lovering 1972). Iron sulfides in these samples are arsenian pyrite and arsenopyrite. Arsenian pyrite formed earlier than arsenopyrite in the paragenetic sequence because arsenopyrite occurs as overgrowth on arsenian pyrite (Fig. 2e). Small amounts of gold-bearing arsenian pyrite and arsenopyrite are enclosed within Fe-poor dolomite (Fig. 2a), whereas a large amount of gold-bearing arsenian pyrite and arsenopyrite is concentrated along jasperoid quartz grain boundaries (Fig. 2b) or disseminated in jasperoid quartz grains (Fig. 2d), where the dolomite was partially or completely dissolved. Lesser amounts of arsenian pyrite replaced biodetritus or fossils in the host rocks, which retain their morphological characteristics (Fig. 2c). The gold-bearing pyrite with As-rich overgrowth zones is commonly observed. The invisible gold content is usually higher in As-rich overgrowth rims on pyrite than in the pyrite cores (Fig. 2e–h).

The textures, crosscutting relations and mineral assemblages of the ores suggest that mineralization in the deposit involved at least four paragenetic stages (Fig. 3). The first stage (stage I) is dominated by disseminated cubic and framboidal pyrite, euhedral ferroan calcite and dolomite, largely of diagenetic origin. Stages II and III are considered to be the main stages for the ore formation. Stage II consists predominately of milky quartz veins with lesser amounts of jasperoid quartz in the host rocks. Some of these veins have orange or gray color due to inclusions of realgar or stibnite, and locally cement ore controlling structures, suggesting that at least some are related to the main mineralization in stage II (Hofstra et al. 2005). Stage III is dominated by iron sulfides, invisible and visible gold, and jasperoid quartz. This stage is expressed as disseminations and veinlets containing (1) early marcasite and arsenian pyrite with elevated contents of invisible gold, along with or within jasperoid quartz and Fe-poor dolomite, and (2) later arsenopyrite, pyrite and native gold grains. Stage IV consists of stibnite, orpiment, and realgar along with dolomite and calcite veins, which occur mainly in the reverse faults that cut the anticline.

Pyrite morphology and texture

Pyrite in the paragenetic sequences described above can be texturally divided into four types according to its morphology under the optical microscopy and in back-scattered electron (BSE) imaging of EMPA. The bioclastic texture is characterized by replacement of biodetritus or fossils by aggregates of small (<10 μm), commonly unzoned arsenian pyrite, which retain their morphological characteristics (Fig. 2c). The disseminated texture is most common in the host rock matrix. Most pyrite with this texture consists of small unzoned arsenian pyrite (<10 μm) that is enclosed within jasperoid quartz (Fig. 2d) or concentrated along jasperoid quartz grain boundaries. Here the dolomite is completely dissolved (Fig. 2b). Zoned grains consist of As-rich overgrowth on As-poor pyrite core (Fig. 2e–h). The overgrowth rims vary in thickness from 1 to 30 μm with elevated contents of invisible gold. This type of pyrite etched with a solution of $KMnO_4$ in 1:1 H_2SO_4 using the technique of Fleet et al. (1993) and BSE imaging revealed three composite textures: euhedral and subhedral pyrite cores, and concentric zones of As-rich and As-poor bands of pyrite (Fig. 2f, g). The pyrite core commonly has a "porous" appearance, probably due to diagenetic origin or inversion of marcasite to pyrite, which involves an increase in density and decrease in volume (Murowchick 1992). Arsenian pyrite is also present in microveinlets between jasperoid quartz veinlets and ferroan calcite in the host rocks. Su et al. (2008) reported that abundant native gold grains, with diameters of 0.1 to 6 μm, were observed in this type of arsenian pyrite veinlets (as example, see Fig. 2h). These native gold grains are usually present at the edge of

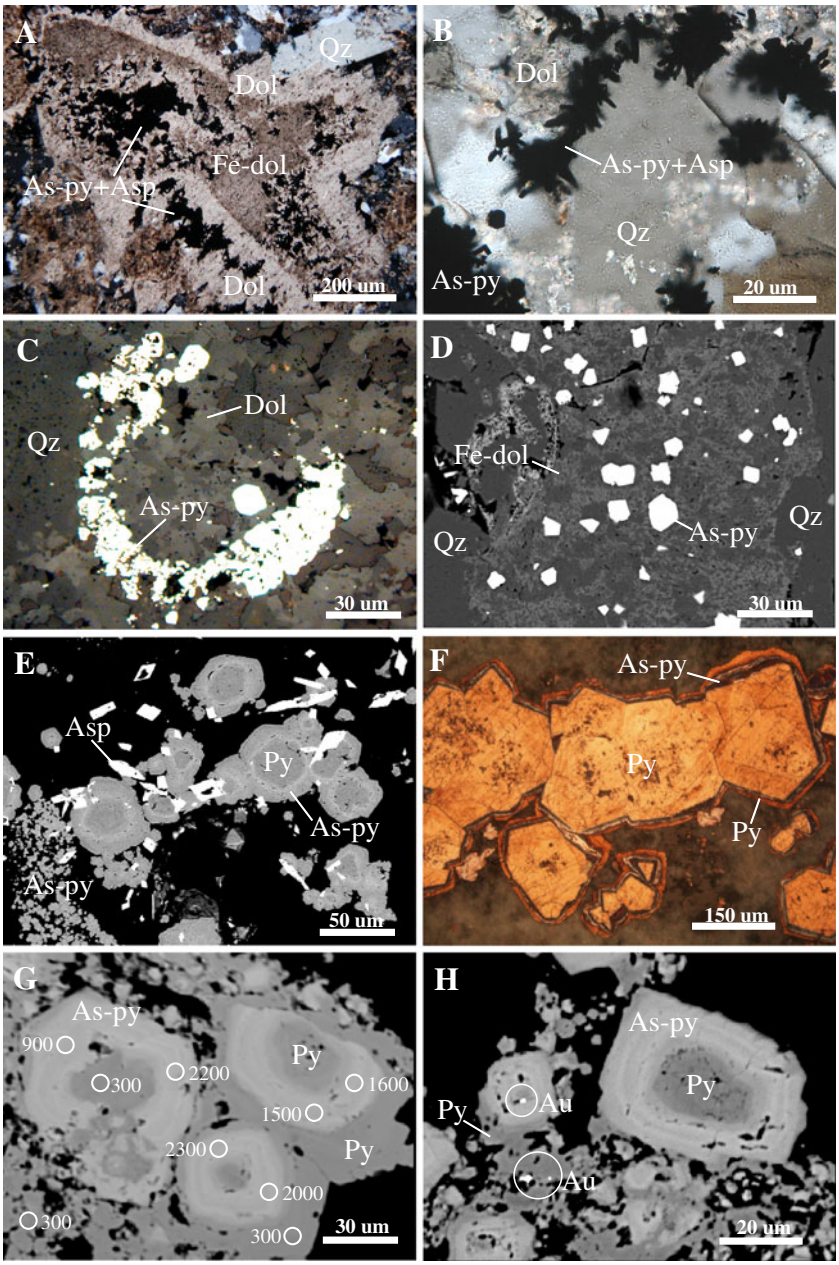

Fig. 2 **a** Transmitted light photomicrograph of the unzoned arsenian pyrite and arsenopyrite co-precipitated with Fe-poor dolomite after dissolution of ferroan dolomite. **b** Transmitted light photomicrograph of gold-bearing arsenian pyrite and arsenopyrite concentrated along the jasperoid quartz grain boundaries. **c** Reflected light photomicrograph of unzoned arsenian pyrite that replaced biodetritus in the host rocks. **d** EMPA back-scattered electron (BSE) image of unzoned arsenian pyrite in jasperoid quartz that contains small relict inclusions of ferroan calcite and dolomite. **e** BSE image of zoned arsenian pyrite and arsenopyrite. **f** Reflected light photomicrograph of zoned arsenian pyrite grains etched with $KMnO_4$ in 1:1 H_2SO_4 solution. *Darker color* indicates zone of arsenic enrichment. **g** BSE image of zoned arsenian pyrite. *Circle* and *number* denote EMPA spot position and concentration of gold (in parts per million), respectively. **h** BSE image of zoned arsenian pyrite and native gold grains that are scattered in hollows of arsenian pyrite crystals or which are present at the edge of As-poor pyrite overgrowth on As-rich pyrite. Abbreviations: *Qz* quartz, *Py* pyrite, *As-py* arsenian pyrite, *Asp* arsenopyrite, *Dol* dolomite, *Fe-dol* ferroan dolomite

As-poor pyrite overgrowth on gold-bearing arsenian pyrite or scattered in hollows of gold-bearing arsenian pyrite crystals that appear to have been corroded (Fig. 2h).

Samples and methodology

The samples of iron sulfides used in this study were examined by ore microscopy and BSE imaging. The potassium permanganate staining technique of Fleet et al. (1993) was applied to reveal pyrite textures. The chemical composition of iron sulfides was analyzed by electron microprobe analysis (EPMA-1600, Shimadu, Japan) with five X-ray wavelength-dispersive spectrometers at the Institute of Geochemistry, Chinese Academy of Sciences. An EDAX energy-dispersive spectrometer was used to identify the native gold grains. Arsenian pyrite and arsenopyrite were analyzed for Fe, S, As, Au, Ag, Sb, Hg, Se, and Co at 25 keV accelerating voltage and 10–40 nA beam current, keeping 10-s counting times. We compared the detection limit for Au using these operating conditions and those used by Palenik et al. (2004) of 25 keV, 40 nA, and a 120-s counting time, and found no significant difference. With our operating conditions, the detection limit of Au in arsenian pyrite is about 300 ppm. For BSE imaging of arsenian pyrite, the beam current was reduced to 4 nA to improve contrast. Standards used were marcasite for Fe and S, GaAs (Alfa, Aesar, USA) for As, pentlandite for Co,

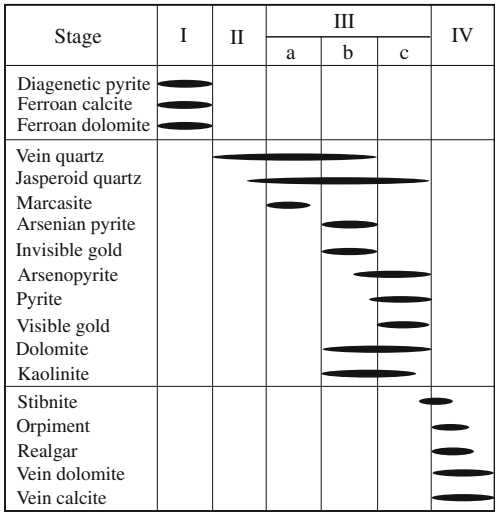

Fig. 3 Paragenetic sequence of the Shuiyindong deposit

stibnite for Sb, and native gold and silver for Au and Ag, respectively.

Gold and arsenic in pyrite and relationship to textures and paragenetic sequences

The concentrations of As, Au, and other trace elements in arsenian pyrite and arsenopyrite were determined using EMPA. The analytical results along with textures are summarized in Table 1 of the Electronic supplementary materials.

Stage-I pyrite consists of disseminated cubic and framboidal pyrite and has a unzoned texture. This type of pyrite has very low arsenic (0.65 to 1.03 wt.% As) and gold contents (below our detection limit of 300 ppm Au) (Table 1).

Stage II is a barren stage before the main mineralization and consists predominantely of milky quartz veins, cut by realgar-orpiment-jasperoid quartz veinlets in the host rocks. Rare iron sulfides were observed in this stage. Stage III is the gold mineralization stage and consists mainly of marcasite, arsenian pyrite, arsenopyrite, and invisible and visible gold. Most of this pyrite variant occurs disseminated and with zoned textures. Three generations of iron sulfides in this stage were identified. The first generation (IIIa) is marcasite with lath-shaped or subhedral grains. Marcasite has moderate arsenic (1.32–2.03 wt.% As), and gold content, commonly below the EMPA detection limit (Table 1). Arsenian pyrite is assigned to the second generation (IIIb) because it usually overgrows the first generation of pyrite or marcasite. This type of pyrite has unzoned and zoned textures. The unzoned arsenian pyrite contains 3.37 to 13.5 wt.% As and 400 to 3,800 ppm Au (Table 1). The highest content of As (up to 32.4 wt.%) was obtained from this generation of pyrite that occurs as tiny grains (1–2 μm) encapsulated in unzoned arsenian pyrite. The zoned arsenian pyrite consists of an As-poor pyrite core and As-rich overgrowth. The overgrowth has higher contents of As (5.02–14.1 wt.%) and Au (800–4,000 ppm) (Table 1). The third generation (IIIc) consists of arsenopyrite and pyrite. Arsenopyrite forms as isolated acicular or lath crystals, aggregates and "saw-like" overgrowth on arsenian pyrite (Fig. 2b, e). Tiny acicular arsenopyrite (2–10 μm) contains 700–1,500 ppm Au, slightly higher than that of arsenopyrite laths (300–1,000 ppm Au) (Table 1). Potassium permanganate staining and BSE imaging of pyrite from this generation reveal that it usually forms euhedral or subhedral crystals overgrown on arsenian pyrite (Fig. 2f, g and h). This pyrite has low As (0.7–1.24 wt.%) and Au (300–600 ppm Au) content (Table 1).

Besides Au and As, arsenian pyrite also contains Co, varying from 0.03–0.05 wt.% (Electronic supplementary materials). There is an antithetic correlation of As with S in arsenian pyrite, regardless of its texture (Fig. 4a). In the Fe–S–As diagram (Fig. 4d, e), all data of arsenian pyrite with variable gold content plot in a zone parallel to the S–As axis, indicating substitution of As for S in the pyrite structure (Fleet and Mumin 1997; Reich et al. 2005; Deditius et al. 2008). In the Au–As plot, all arsenian pyrite data fall below the solubility limit of gold for arsenian pyrite (Fig. 4b)

Table 1 Summary of EMPA results of Au and As in arsenian pyrite and arsenopyrite, along with texture from Shuiyindong deposit

Stage	Mineral assemblage	Pyrite size (μm)	Pyrite morphology	Ore texture	As content (wt.%)	Au content (ppm)	As and Au distribution
Stage I	Diagenetic frambodial pyrite	>20	Euhedral	FGD	0.65–1.03	<300	n.d.
Stage III	Pyrite or marcasite core	10–200	Subhedral	Porous core	1.32–2.03	<300	n.d.
	Arsenian pyrite	1–30	Subhedral–euhedral	Overgrowth	5.02–14.1	800–4,000	Homogeneous
	Pyrite	>10	Euhedral	Overgrowth	0.70–1.24	300–600	n.d.
	Unzoned arsenian pyrite	1–10	Subhedral–euhedral	FGD	3.37–13.5	400–3,800	Homogeneous
	Acicular arsenopyrite	2–10	Acicular	FGD	42.43–46.69	700–1,500	n.d.
	Lath arsenopyrite	>10	Lath	FGD	41.54–47.22	300–1,000	n.d.

FGD fine-grained disseminated, *n.d.* not determined

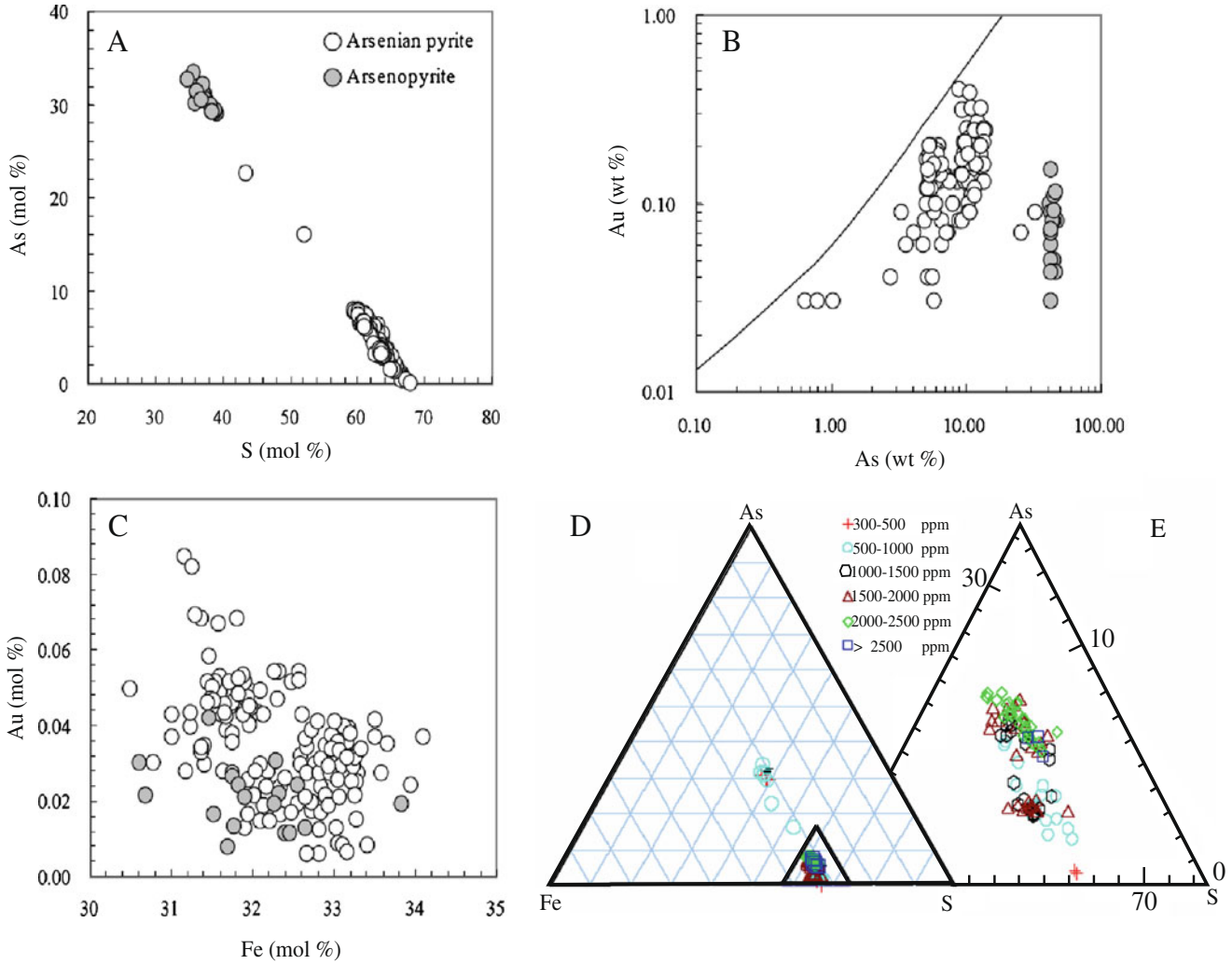

Fig. 4 Correlation among Fe, S, As, and Au in arsenian pyrite. The *line* in (**b**) is the inferred solubility limit of gold for arsenian pyrite as documented by Reich et al. (2005)

(Reich et al. 2005), indicating that they formed from solutions undersaturated with gold (Simon et al. 1999a; Reich et al. 2005). In contrast, there is no clear correlation between Fe and Au in arsenian pyrite (Fig. 4c). No correlation is observed among Co, Sb, and Au. The EMPA maps of representative grains of zoned arsenian pyrite (Fig. 5a) show that the rim has relatively homogeneous distribution of As and Au (Fig. 5b, c), with 11.2 to 14.1 wt.% As and 1,600 to 2,500 ppm Au, respectively, suggesting that gold in the rim is likely present as Au^{1+} in a structurally bound Au complex of the type proposed by Simon et al. (1999b).

Discussion

Geochemistry of gold-bearing arsenian pyrite

The presence of As and Au in pyrite has been widely recognized in natural arsenian pyrite and marcasite from Carlin-type and epithermal gold deposits (Bakken et al. 1989; Cook and Chryssoulis 1990; Simon et al. 1999a, b; Cline 2001; Emsbo et al. 2003; Zhou and Wang 2003), and laboratory syntheses (Clark 1960; Kretschmar and Scott 1976; Fleet and Mumin 1997). The maximum solubility of As and chemical state of gold in iron sulfide minerals remain controversial (Clark 1960; Kretschmar and Scott 1976; Mao 1991; Arehart et al. 1993; Fleet et al. 1993, 1997; Li et al. 2003; Reich et al. 2005). Using spectroscopic measurements (XANES and EXAFS) and microanalysis (SIMS), Simon et al. (1999a,b) concluded that gold in arsenian pyrite occurs in solid solution (Au^{1+}) and as nanoparticles of native gold (Au^{0}). Palenik et al. (2004) have located regions containing large concentrations of gold nanoparticles (5–10 nm) in As-rich overgrowths on pyrite from the Screamer deposit in the Carlin trend, using high-resolution transmission electron microscopy, and proposed two possible origins for gold nanoparticles in arsenian pyrite: (1) gold exceeds its solubility limit in

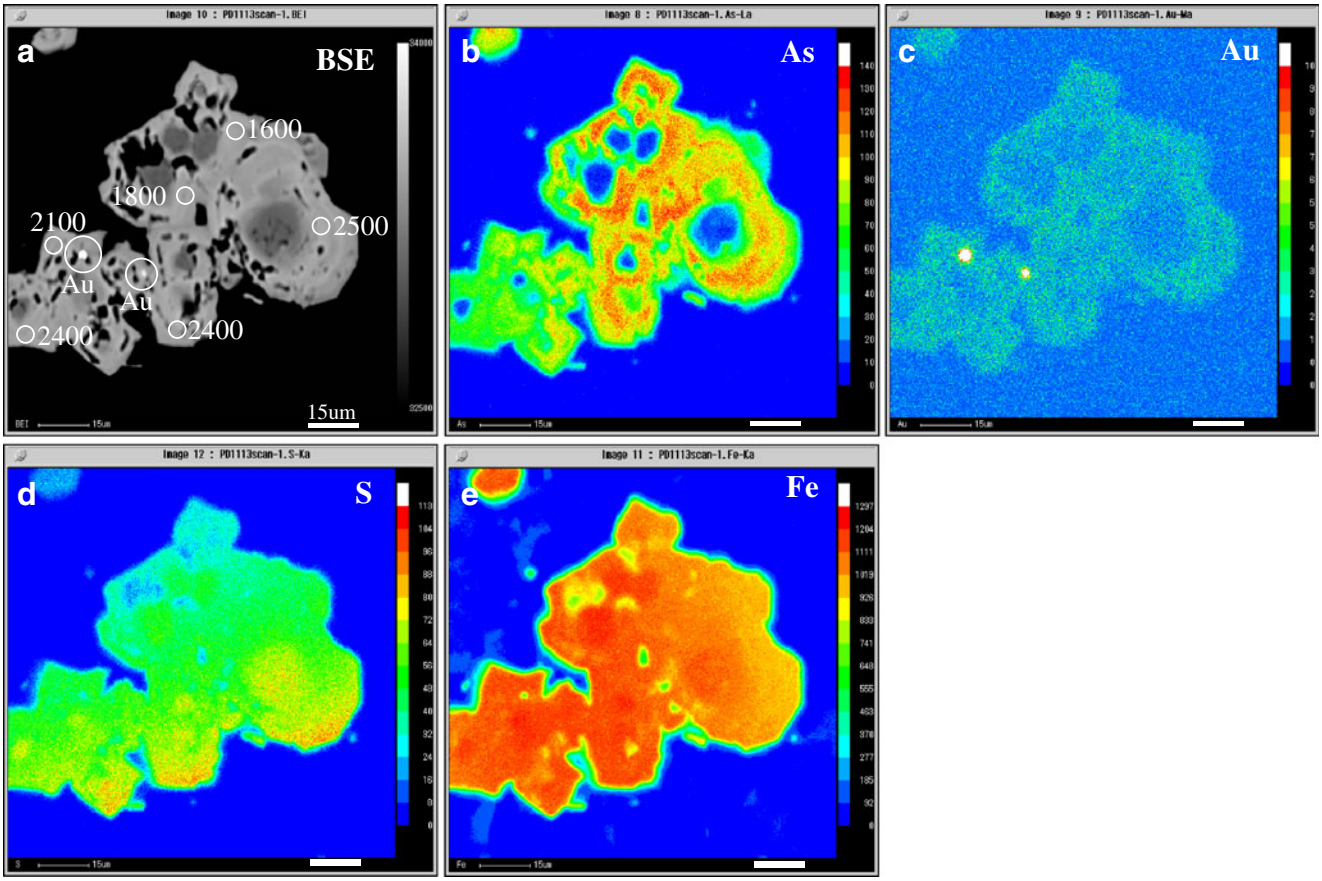

Fig. 5 EMPA-BSE image of arsenian pyrite and maps of arsenic, gold, sulfur, and iron in arsenian pyrite showing invisible and visible gold and its relation to surrounding arsenian pyrite. Note the relatively homogeneous distribution of As and Au in arsenian pyrite, and two native gold grains in (**a**) and (**c**) scattered in hollows of gold-bearing arsenian pyrite. *Circles* and *numbers* in (**a**) denote the EMPA spot position and concentration of gold (in parts per million), respectively

arsenian pyrite; and (2) exsolution of native metal from metastable arsenian pyrite was caused by a later event in the history of the deposit. Reich et al. (2005) further determined a solubility limit for gold in arsenian pyrite, using SIMS and EMPA data.

In this study, we suggest that gold in arsenian pyrite is present in two forms in the Shuiyindong Carlin-type gold deposit:

1. As-rich overgrowth rims on pyrite. The relatively homogeneous distribution and a positive correlation of As and Au, with Au/As ratios plotting below the solubility limit of gold for arsenian pyrite, indicate that invisible gold is likely present as Au^{1+} in a structurally bound Au complex in arsenian pyrite as proposed by Simon et al. (1999b). The chemical zonation of pyrite in the Shuiyindong deposit reflects the chemical evolution of the ore-bearing fluids. The early ore fluids would have relatively high activities of As and Au, to deposit unzoned and zoned arsenian pyrite that host most gold in the deposit. The ore fluids then became depleted in Au and As and formed As-poor pyrite overgrowth rims on gold-bearing arsenian pyrite.
2. The second style is composed of submicrometer- or nanometer-sized native gold that is present at the edge of As-poor pyrite overgrowths on arsenian pyrite or scattered in hollows of arsenian pyrite crystals that appear to have been corroded (Fig. 5a, c), suggesting that they formed when gold-bearing arsenian pyrite reverted to gold-poor arsenian pyrite and native gold (Simon et al. 1999a), or may result from incursion of relatively acidic or oxidized fluids that were able to dissolve gold-bearing arsenian pyrite and remain saturated with gold (Su et al. 2008).

Geochemical modeling of ore fluid composition and speciation

The LA-ICP-MS data of fluid inclusions by Su et al. (2009a) allow to evaluate the speciation of Au and other elements and the saturation indices of Au in the ore-forming fluid by geochemical modeling. The solubility and speciation of elements in the ore fluid was modeled by using the code PHREEQC (Parkhurst and Appello 1999) with

our own thermodynamic database compiled for this study. For modeling, the standard states for the solids are defined as unit activity for pure solids at the temperature and pressure of interest. The standard state for water is the unit activity of pure water. For aqueous species other than H_2O, the standard state is the unit activity of the species in a hypothetical one molal ideal solution referenced to infinite dilution at the temperature and pressure of interest.

In ore-forming fluids, the most likely ligands for complexation with Au^+ are HS^-, Cl^-, and OH^- (Stefansson and Seward 2003a). The thermodynamic data for Au chloride complexes are provided by Sverjensky et al. (1997). Equilibrium constants for $Au(HS)_2^-$ and $AuHS_{(aq)}^0$ were taken from Benning and Seward (1996), in which the solubility of gold in aqueous sulfide solutions was measured at temperatures of 150°C to 500°C and pressure of 500 to 1,500 bars. Since the $Au(OH)_2^-$ complex is predominant at pH>12 (Vlassopoulos and Wood 1990), $AuOH_{(aq)}^0$ was the only Au hydroxyl complexes considered in our study. Stefansson and Seward (2003b) provided equilibrium constants for $AuOH^0$ from 25°C to 600°C and 500 to 2,000 bars. For arsenic aqueous complexes, the equilibrium constants were calculated with the SUPCRT92 software (Johnson et al. 1992) by employing the thermodynamic properties from Marini and Accornero (2007). The equilibrium constants used in the calculations are listed in Table 2 of the Electronic supplementary materials. Others not listed are from the LLNL database (Wolery 1992).

The total concentrations of elements in the PHREEQC input file were based on the LA-ICP-MS analysis results of fluid inclusion sample SYD035-Q2. The pH value was determined by 2 mol% CO_2 in the inclusion fluid and the calculation results in pH about 4. Because no H_2S concentration was provided by the LA-ICP-MS analysis, 0.1 M H_2S was assumed following Hofstra et al. (1991). The model temperature was 220°C and pressure was 750 bars.

The speciation calculations show that the dominant Au species are $Au(HS)_2^-$ (77%) and $AuHS_{(aq)}^0$ (23%). The hydroxyl and chloride complexes $Au(OH)_{(aq)}^0$, $AuCl_3^{-2}$, $AuCl_2^-$, $AuCl_{(aq)}^0$ are negligible. The ore fluid is undersaturated with respect to native Au, with a saturation index of −3.8. The predominant As species is $H_3AsO3_{(aq)}^0$. Cu, Pb, Ag, and Fe form aqueous complexes primarily with chloride. Antimony is mostly in the form of Sb hydroxide complexes.

Deposition of gold in arsenian pyrite and implications for the formation of Carlin-type gold deposits

Numerous studies of Carlin-type deposits in Nevada have concluded that gold-rich arsenian pyrite precipitated from H_2S-rich fluids, which sulfidized iron-bearing minerals in the host rocks (Hofstra et al. 1991; Hofstra and Cline 2000; Kesler et al. 2003). Recent studies of fluid inclusions at Shuiyindong showed that the ore-forming fluids are rich in CO_2 (2–4 mol%) with low salinity at a temperature of 220± 20°C, and have high contents of the characteristic ore elements (120 ppm As, 20 ppm Sb, and 3–5 ppm Au) but are poor in Fe (below 400 ppm Fe: Su et al. 2009a). Iron in sulfide minerals was probably derived from dissolution of ferroan carbonate minerals (with up to 7.0 wt.% Fe determined by EMPA: Su et al. 2008) in the host rocks, based on petrographic observations (Fig. 2a–d), by such as the following reaction (where $x \leq 1$):

$$H_2CO_3 + 2Cl^- + \left(Ca_{(1-x)}, Fe_{(x)}\right)CO_3 = (1-x)CaCl_{2(aq)} + xFeCl_{2(aq)} + 2HCO_3^-$$

This reaction may be representative of decarbonation of the host rocks in Carlin-type systems, which provides the main source of iron for sulfidation during gold deposition, as is evidenced by small relict inclusions of ferroan calcite or dolomite in jasperoid quartz (Fig. 2b, d). Sulfidation of dissolved iron by H_2S-rich ore fluids containing $Au(HS)_2^-$ or $Au(HS)^0$ (Seward 1973, 1991), along with arsenic as $H_3AsO_{3(aq)}$ complex (Heinrich and Eadington 1986; Pokrovski et al. 2002), such as determined from the geochemical modeling calculations above, could deposit gold-bearing arsenian pyrite, possibly by the following reaction:

$$2Fe^{+2} + 2H_3AsO_{3(aq)}^0 + H_2S_{(aq)} + 2\left[Au(HS)_2\right]^-_{(aq)} + H_{2(g)} = Fe(S,As)_2Au_2{\cdot}S^0 + FeS_2 + 2H^+ + 6H_2O$$

This reaction is strongly dependent on the activity of reduced sulfur (as H_2S or HS^-), and a decrease in H_2S produced by sulfidation would promote the formation of arsenian pyrite that hosts most gold in the deposit. The reaction involves reduction of As (3+) and Au (1+) by consumption of $H_{2(g)}$ which can be provided by reaction of the metal-transporting fluids with the local organic-rich sediments (Su et al. 2009a). Such a reaction also can explain the petrographic observations that As-poor pyrite is overgrown on gold-bearing arsenian pyrite (Fig. 2g, h). In response to the dissolution of carbonates from the host rocks, calcium to magnesium ions could be retained in the fluids and deposited in the form of Fe-poor calcite or dolomite veins or veinlets, as commonly observed in the Shuiyindong district (Su et al. 2008, 2009b).

Hydrogen and oxygen isotope compositions of ore fluids (δD=−56‰ to −68‰, $\delta^{18}O$=4‰ to 16.5‰: Su et al. 2009a), and sulfur isotope compositions of ore-stage pyrite ($\delta^{34}S$=3.2‰ to 7‰: Liu and Liu 2005) at Shuiyindong indicate dominantly metamorphic water and a sedimentary

source of sulfur, but a deep magmatic component cannot be excluded, possibly related to crustal thickening and prograde metamorphism during the late Yanshanian orogeny. The metamorphic fluids with high contents of the characteristic ore elements (As, Sb, Au, and possibly S) discharged along the unconformity between the Maokou Limestone and the Longtan Formation at Shuiyindong, reacted with iron-carbonate and carbon-rich sedimentary host rocks, to deposit arsenian pyrite and arsenopyrite that host most of the gold in the deposit. Therefore, fluid reduction and sulfidation of wall-rock iron by H_2S-rich ore fluids are proposed to be the most important mechanisms for the formation of auriferous arsenian pyrite in the Shuiyindong deposit, as suggested for Carlin-type deposits elsewhere (Hofstra et al. 1991; Hofstra and Cline 2000; Kesler et al. 2003).

Conclusions

There are four different types of gold-bearing arsenian pyrite in the paragenetic sequence of hydrothermal mineralization at the Shuiyindong deposit. Pyrite and marcasite occur as disseminations and the core of zoned pyrite contains the lowest amount of Au and As, whereas tiny unzoned arsenian pyrite and As-rich zoned arsenian pyrite crystals have the largest amount of Au and As. Arsenopyrite and pyrite overgrowth rims on the zoned arsenian pyrite also contain lower contents of Au. The negative correlation of As and S in arsenian pyrite is consistent with the substitution of As for S in the pyrite structure.

Gold is present in arsenian pyrite in two forms. Invisible gold occurs in As-rich overgrowth on preexisting pyrite. The relatively homogeneous distribution and a positive correlation of As and Au, with Au/As ratios below the solubility limit of gold in arsenian pyrite, suggest that this gold is likely present as Au^{1+} in a structurally bound Au complex and formed from fluids undersaturated with gold. Another form is composed of submicrometer- and nanometer-size native gold grains. They are usually present at the edge of As-poor pyrite overgrowth on the As-rich pyrite or are scattered in hollows of arsenian pyrite crystals that appear to have been corroded, suggesting that they formed later than gold-bearing arsenian pyrite and were the product of remobilization of gold-bearing arsenian pyrite or direct precipitation of native gold.

The chemical zonation of pyrite in the Shuiyindong deposit reflects the chemical evolution of the ore fluids. The zoned arsenian pyrite likely formed from a fluid with relatively high activity of As to Au during an early stage. Later, the ore fluids developed to Au- and As-poor fluids to form As-poor pyrite overgrowth on gold-bearing arsenian pyrite. Arsenopyrite overgrowth on arsenian pyrite is interpreted to be caused by the input of another later fluid with relatively high activity of As. The lack of evidence of boiling and the low iron content of fluid inclusions in quartz suggest that the iron in arsenian pyrite was most likely derived from dissolution of ferroan minerals in the host rocks, especially from ferroan carbonates, with sulfidation of the dissolved iron by H_2S-rich ore fluids being the most important mechanism of gold deposition in the Shuiyindong deposit.

Acknowledgments We are grateful to the Guizhou Zijin Gold mine for access to the mine and to Jianzhong Liu and Chuanqin Liu for geological guidance and discussion during fieldwork. Dr. Guofu Zhou is appreciated for his assistance with the electron microprobe analysis. Review comments by Professor Meifu Zhou improved presentation and scientific arguments. Editor Bernd Lehmann, Martin Reich, and an anonymous referee are thanked for their thoughtful and thorough reviews. The project was financially supported by the National Science Foundation of China (grant nos. 40672067 and 40972072), State Key Basic Research Program of China (grant no. 2007CB411402), and the Foundation of State Key Laboratory of Ore Deposit Geochemistry (grant no. KCZX2009).

References

Arehart GB, Chryssoulis SL, Kesler SE (1993) Gold and arsenic in iron sulfides from sediment-hosted disseminated gold deposits: implications for depositional processes. Econ Geol 88:171–185

Bakken BM, Hochella MF, Marshall AF, Turner AM (1989) High-resolution microscopy of gold in unoxidized ore from the Carlin Mine, Nevada. Econ Geol 84:171–179

Benning LG, Seward TM (1996) Hydrosulphide complexing of Au(I) in hydrothermal solutions from 150–400°C to 500–1500 bar. Geochim Cosmochim Acta 60:1849–1871

Clark LA (1960) The Fe-As-S system: phase relations and applications. Econ Geol 55:1345–1381

Cline JS (2001) Timing of gold and arsenic sulfide mineral deposition at the Getchell Carlin-type gold deposit, north-central Nevada. Econ Geol 96:75–89

Cook NJ, Chryssoulis SL (1990) Concentrations of invisible gold in the common sulfides. Can Miner 28:1–16

Deditius AP, Utsunomiya S, Renock D, Ewing RC, Ramana CV, Becker U, Kesler SE (2008) A proposed new type of arsenian pyrite: composition, nanostructure and geological significance. Geochim Cosmochim Acta 72:2919–2933

Emsbo P, Hofstra AH, Lauha EA, Griffin GL, Hutchinson RW (2003) Origin of high-grade gold ore, source of ore fluid components and genesis of the Meikle and neighboring Carlin-type deposits, north Carlin Trend, Nevada. Econ Geol 98:1069–1105

Fleet ME, Mumin AH (1997) Gold-bearing arsenian pyrite and marcasite and arsenopyrite from Carlin trend gold deposits to laboratory synthesis. Am Miner 82:182–193

Fleet ME, Chryssoulis SL, MacLean PJ, Davidson R, Weisener CG (1993) Arsenian pyrite from gold deposits: Au to As distribution investigated by SIMS and EMP and color staining and surface oxidation by XPS and LIMS. Can Miner 31:1–17

Fu SH, Gu X, Wang Q, Xia Y, Zhang XC, Tao Y (2004) The typomorphic characteristics of gold-bearing pyrites from Shuiyindong gold deposit, SW Guizhou. Acta Miner Sin 24:75–80 (in Chinese with English abstract)

Heinrich CA, Eadington PJ (1986) Thermodynamic predictions of the hydrothermal chemistry of arsenic, cassiterite-arsenopyrite-base metal sulfide deposits. Econ Geol 81:511–529

Hofstra AH, Cline JS (2000) Characteristics and models for Carlin-type gold deposits. Rev Econ Geol 13:163–220

Hofstra AH, Leventhal JS, Northrop HR, Landis GP, Rye RO, Birak DJ, Dahl AR (1991) Genesis of sediment-hosted disseminated gold deposits by fluid mixing and sulfidization: chemical-reaction-path modeling of ore-depositional processes documented in the Jerritt Canyon district, Nevada. Geology 19:36–40

Hofstra AH, Zhang XC, Emsbo P, Hu RZ, Su WC, Christiansen WD, Fu SW, Theodorakos P (2005) Source of ore fluids in Carlin-type gold deposits in the Dian-Qian-Gui area and West Qinling belt, P. R. China: Implications for genetic models. In: Mao JW, Bierlein FP (eds) Mineral Deposits Research: Meeting the Global Challenge, vol 1. Heidelberg, Springer, pp 533–536

Johnson JW, Oelkers EH, Helgeson HC (1992) SUPCRT92: a software package for calculating the standard molal thermodynamic properties of minerals, gases, aqueous species, and reactions from 1 to 5000 bar and 0°C to 1000°C. Comput Geosci 18:899–947

Kesler SE, Fortuna J, Ye ZJ, Alt JC, Zohar DP, Borhauer J, Chryssoulis SL (2003) Evaluation of the role of sulfidation in deposition of gold, Screamer section of the Betze-Post Carlin-type deposit, Nevada. Econ Geol 98:1137–1157

Kretschmar U, Scott SD (1976) Phase relations involving arsenopyrite in system Fe-As-S and their application. Can Miner 14:364–386

Li JL, Qi F, Xu QS (2003) A negatively charged species of gold in minerals—further study of chemically bound gold in arsenopyrite and arsenian pyrite. N Jb Miner Monatsh 5:193–214

Liu JZ (2001) The geology of the Yanshang gold deposit, Zhenfeng county, Guizhou. Guizhou Geol 18:174–178 (in Chinese with English abstract)

Liu JZ (2003) Ore characteristics and gold occurrence of the Shuiyindong gold deposit, Guizhou. Guizhou Geol 20:30–34 (in Chinese with English abstract)

Liu JZ, Liu CQ (2005) Origin and metallogenic model for Shuiyindong gold deposit of Guizhou. Guizhou Geol 22:9–13 (in Chinese with English abstract)

Lovering TG (1972) Jasperoid in the United State—its characteristics, origin, and economic significance. US Geol Surv Prof Pap 710:1–164

Mao SH (1991) Occurrence and distribution of invisible gold in a Carlin-type gold deposit in China. Am Miner 76:1964–1972

Marini L, Accornero M (2007) Prediction of the thermodynamic properties of metal-arsenate and metal-arsenite aqueous complexes to high temperatures and pressures and some geological consequences. Environ Geol 52:1343–1363

Murowchick JB (1992) Marcasite inversion and the petrographic determination of pyrite and ancestry. Econ Geol 87:1141–1152

Palenik CS, Utsunomiya S, Reich M, Kesler SE, Wang LM, Ewing RC (2004) "Invisible" gold revealed: direct imaging of gold nanoparticles in a Carlin-type deposit. Am Miner 89:1359–1366

Parkhurst DL, Appello AAJ (1999) User's Guide to PHREEQC (version 2)—A computer program for speciation, batch-reaction, one-dimensional transport, and inverse geochemical modeling. Water-Resource Investigation Report, U.S. Geological Survey, Reston. pp. 99–4259

Pokrovski GS, Kara S, Roux J (2002) Stability and solubility of arsenopyrite, FeAsS, in crustal fluids. Geochim Cosmochim Acta 66:2361–2378

Reich M, Kesler SE, Utsunomiya S, Palenik CS, Chryssoulis SL, Ewing RC (2005) Solubility of gold in arsenian pyrite. Geochim Cosmochim Acta 69:2781–2796

Seward TM (1973) Thio complexes of gold and the transport of gold in hydrothermal ore solutions. Geochim Cosmochim Acta 37:370–399

Seward TM (1991) The hydrothermal geochemistry of gold. In: Foster RP (ed) Gold metallogeny and exploration. Blackie, Glasgow, pp 37–62

Simon G, Kesler SE, Chryssoulis S (1999a) Geochemistry and textures of gold-bearing arsenian pyrite, Twin Creeks, Nevada: implications for deposition of gold in Carlin-type deposits. Econ Geol 94:405–422

Simon G, Huang H, Penner-Hahn JE, Kesler SE, Kao L (1999b) Oxidation state of gold and arsenic in gold-bearing arsenian pyrite. Am Miner 84:1071–1079

Stefansson A, Seward TM (2003a) Stability of chloridogold(I) complexes in aqueous solutions from 300 to 600°C and from 500 to 1800 bar. Geochim Cosmochim Acta 67:4559–4576

Stefansson A, Seward TM (2003b) The hydrolysis of gold(I) in aqueous solutions to 600°C and 1500 bar. Geochim Cosmochim Acta 67:1677–1688

Su WC, Xia B, Zhang HT, Zhang XC, Hu RZ (2008) Visible gold in arsenian pyrite at the Shuiyindong Carlin-type gold deposit, Guizhou, China: implications for the environment and processes of ore formation. Ore Geol Rev 33:667–679

Su WC, Heinrich CA, Pettke T, Zhang XC, Hu HR, Xia B (2009a) Sediment-hosted gold deposits in Guizhou, China: products of wall-rock sulfidation by deep crustal fluids. Econ Geol 104:73–93

Su WC, Hu RZ, Xia B, Xia Y, Liu YP (2009b) Calcite Sm-Nd isochron age of the Shuiyindong Carlin-type gold deposit, Guizhou, China. Chem Geol 258:269–274

Sverjensky DA, Shock EL, Helgeson HC (1997) Prediction of the thermodynamic properties of aqueous metal complexes to 1000°C and 5 kb. Geochim Cosmochim Acta 61:1359–1412

Vlassopoulos D, Wood SA (1990) Gold speciation in natural-waters. 1. Solubility and hydrolysis reactions of gold in aqueous-solution. Geochim Cosmochim Acta 54:3–12

Wolery TJ (1992) A software package for geochemical modeling of aqueous systems: package overview and installation guide (version 7.0): URCL-MA-110662-PT-I, Lawrence Livermore Laboratory, California University, Livermore, CA

Zhou YQ, Wang KR (2003) Gold in the Jinya Carlin-type deposit: characterization and implications. J Min Mater Charact Eng 2:83–100